Monolayer Level Depth Profiling by Laser Induced Fluorescence Spectroscopy

Xing-Zheng Wu, Takehiko Kitamori, Norio Teramae,† and Tsuguo Sawada*
Department of Industrial Chemistry, Faculty of Engineering, The University of Tokyo,
7-3-1 Hongo, Bunkyo, Tokyo 113
†Department of Applied Chemistry, Faculty of Engineering, Nagoya University,
Hurouchou 1, Chigusaku, Nagoya 464
(Received January 28, 1991)

Application limits of the proposed concentration depth profile using laser induced fluorescence spectroscopy based on the reciprocal principle (*Bull. Chem. Soc. Jpn.*, **64**, 755 (1991)) were investigated. Although this method has no limitations regarding film thickness and spatial resolution in the depth direction theoretically, for practical applications, they are limited by the instrumental factors. Effects of uncertainty in the observation angle measurement, which depends on the size of the detector, the mechanical precision of the rotating stage, and experimental errors in the fluorescence intensity measurement on the accuracy of the reconstructed concentration depth profile were discussed in detail. The theoretical results predicted nanometer level depth profiling with our laboratory-constructed instruments. A 29 nm thick model film sample, consisting of long chain molecular bilayers, was used to verify the theoretical analysis results. The concentration depth profile for bilayer level steps of about 5 nm was obtained under our experimental conditions. Possible improvements in this method and monolayer level depth profiling were also considered.

Many problems in thin film chemistry and materials science are concerned with the distribution of chemical species in the depth direction.[1,2] In many situations, vacuum spectroscopic depth profiling methods are undesirable, because they are destructive methods and they need high vacuum conditions which are unsuitable for in situ and in vivo analysis. Optical spectroscopical concentration depth profiling methods such as photoacoustic spectroscopy (PAS) depth profiling,[3] attenuated total reflection (ATR) spectroscopy depth profiling[4] are non-destructive and non-contact methods not requiring high vacuum system.[5,6] Recently, we have reported on the concentration depth profiling technique using laser induced fluorescence spectroscopy under normal incidence conditions based on the reciprocal principle.[7] Using this method, the quantitative concentration depth profile of a 187 nm thick Langmuir–Blodgett (LB) model film sample was obtained by the least square method. This spectroscopic technique is attractive since it has a high spatial resolution in the depth direction and can be used on a film sample thinner than the wavelength of the excitation light. In addition, by using the normal incidence conditions, it is possible to obtain a three dimensional concentration profile by scanning the excitation beam.

However, to function as a basic methodology for practical applications, answers must be got for the following questions: How accurate is the reconstructed concentration depth profile? Is there any limitation to film thickness for this method? What is the spatial resolution in the depth direction? Then it is necessary to investigate the application limits.

In this paper, we investigate application limits, such as film thickness, and accuracy of the reconstructed concentration depth profile by this method. The main instrumental error sources such as the uncertainty in determining observation angle, the mechanical precision of the rotating stage, and the uncertainty in the fluorescence intensity measurement, and their effects on the accuracy of the reconstructed concentration depth profile are discussed. In the experiments, a 29 nm thick LB model film sample where fluorophore is distributed in the form of a nearly linear function is used to verify the theoretical conclusions, and a bilayer level concentration depth profile is obtained.

Theory and Simulation

The basic theory of depth profiling using laser induced fluorescence spectroscopy under normal incidence conditions based on the reciprocal principle has been discussed in our previous paper.[7] Here we summarize it briefly. Figure 1 illustrates the basic optical arrangement. The fluorescence intensity $F(\theta)$ obtained

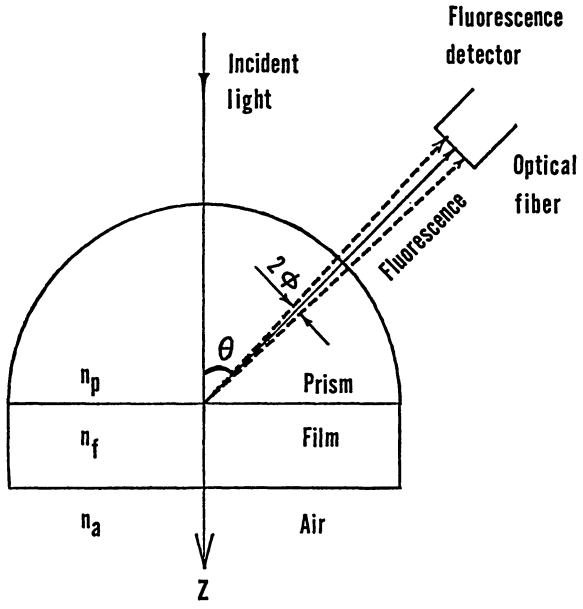

Fig. 1. Measurement principle of the depth profiling method.

at an observation angle θ under normal incidence conditions can be expressed as Eq. 1,

$$F(\theta)=k\int_0^t C(z)T(\theta, z)\mathrm{d}z, \quad (1)$$

where $C(z)$ is the concentration distribution in the depth direction z, t is the thickness of the sample, and k is a constant given by material constants and instrumental factors. The transmission function $T(\theta, z)$ can be obtained by theoretical analysis of multiple reflection of the fluorescence electromagnetic wave between prism/film and film/air interfaces.[8] When θ, z, and t are given, $T(\theta, z)$ can be calculated exactly from the optical parameters such as the fluorescence wavelength and the refractive indices of the prism, film, and air. Thus $C(z)$ can be obtained by resolving the inverse integral of Eq. 1 from a set of fluorescence intensity data. It is well known that resolution of the inverse integral problem is difficult due to the ill-posed problem.[9–11] However, for the present method, if a process leading to the formation of $C(z)$ is estimated beforehand, then $C(z)$ can be easily obtained by the least square method.[7] As shown in the previous experimental reports of this depth profiling method,[7] the experimental errors seriously affect results of the reconstructed concentration profiles. We can discuss the effects of the instrumental error factors on the accuracy and the limitation of the present depth profiling method by a numerical simulation method. Since $C(z)$ is obtained from a set of fluorescence intensities determined at a series of observation angles by the least square method, the following three error sources are considered. First, uncertainty ϕ in observation angle, as shown in Fig. 1, is determined by the size of the detector and the distance between the detector and the illuminated point. Second, the angular error $\Delta\theta$ is determined by the mechanical precision of the rotating stage. Third, the measurement error ΔF in the fluorescence intensity is caused by noise such as electric noise. An influence of base-line drift on ΔF cannot be disregarded, when measurement period is relatively longer than the instrument stability.

Here, three typical concentration distribution cases are discussed. In the first case, $C(z)$ is a linear function form

$$C(z)=Az+B \quad (2)$$

as shown in Fig. 2-A), which was used as a trial function in our previous paper.[7] In the second case, $C(z)$ is an exponential function form

$$C(z)=C_0\exp(-z/l) \quad (3)$$

as shown in Fig. 2-B), which often emerges in chemical kinetics systems. In the third case, $C(z)$ is an error function form

$$C(z)=C_0[1-\mathrm{erf}(-z/l)] \quad (4)$$

as shown in Fig. 2-C), which is usually met in a diffusion limiting process. The parameters A, B, C_0, l can be obtained by the least square method, i. e., by

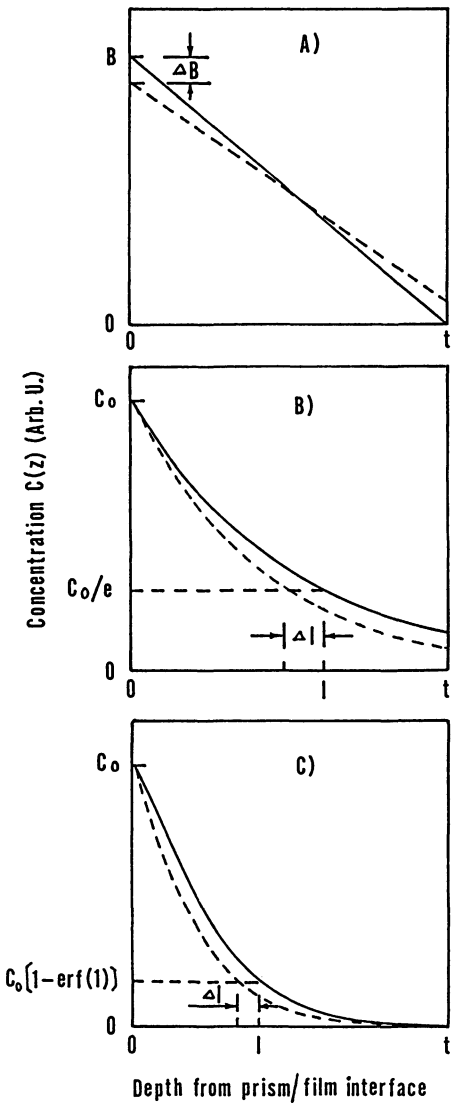

Fig. 2. Model function used in the simulation. The solid and dashed lines represent the original $C(z)$ and reconstructed $C(z)$. A: $C(z)$ is a linear function form. B: $C(z)$ is an exponential function form. C: $C(z)$ is an error function form.

minimizing the following value s,

$$s=\sum_i[F_m(\theta_i)-F_c(\theta_i)]^2/g_{\theta_i}, \quad (5)$$

where i means the i-th measurement data, $F_m(\theta_i)$ and $F_c(\theta_i)$ are the measured and calculated fluorescence intensities, respectively, and g_{θ_i} is a weight factor.

The differences between actual and calculated values of parameters A, B, and l are represented by ΔA, ΔB, and Δl, respectively (Fig. 2). The accuracy of the reconstructed $C(z)$ is evaluated by the relative errors of the parameters in Eqs. 2—4, i. e., $\Delta A/A$ or $\Delta B/B$ for the linear distribution case, and $\Delta l/l$ for the exponential and error function cases.

In this simulation, θ_i is assumed to be varied from 20° to 80° with 1° steps. The calculated fluorescence intensities $F_c(\theta_i)$ in Eq. 5 are obtained according to Eq. 1 for

the above three cases expressed as Eqs. 2—4. The constants in Eqs. 2—4 are normalized as follows: A (% nm^{-1}) and B (%) are $-1(\%)/t(\mathrm{nm})$ and 1(%), respectively, and C_0 (%) and l (nm) are 1(%) and t (nm), respectively. In order to calculate $\Delta A/A$, $\Delta B/B$, and $\Delta l/l$ caused by ϕ, the measured fluorescence intensity $F_m(\theta_i)$ in Eq. 5 is simulated by substituting θ_i with $\theta_i+\phi$. When the effect of $\Delta\theta$ is considered, the observation angle θ_i takes a certain value within the range of $\theta_i\pm\Delta\theta$. In the worst case, θ_i is randomly given by either $\theta_i+\Delta\theta$ or $\theta_i-\Delta\theta$, leading to $F_m(\theta_i+\Delta\theta)$ or $F_m(\theta_i-\Delta\theta)$. Considering ΔF, $F_m(\theta_i)$ in Eq. 5 is within the range of $F_m(\theta_i)\pm\Delta F$, and the value of $F_m(\theta_i)$ in Eq. 5 is also substituted randomly by $F_m(\theta_i)+\Delta F$ or $F_m(\theta_i)-\Delta F$. With these simulated values of $F_m(\theta_i)$, the relative errors of $\Delta A/A$, $\Delta B/B$, and $\Delta l/l$ caused by ϕ, $\Delta\theta$, and ΔF are obtained from Eq. 5. The results are shown in Figs. 5, 6, and 7, respectively.

Experimental

The experimental set up used is the same as reported in our previous paper.[7] An Ar^+ laser (output, 30 mW) provides the excitation light (wavelength, 488 nm). The laser beam was modulated with a chopper. The chopped beam was focused on the focal plane of the hemicylindrical prism (refractive index n, 1.88) which was mounted on two rotating stages. A step index type optical fiber bundle was used to collect the fluorescence transmitted through the prism. The area collecting fluorescence was 0.2 mm×1 mm, and the numerical aperture was 0.57. One end of the optical fiber was fixed at the focal plane of the prism and the other end of the optical fiber was coupled with a monochromator. A film polarizer was placed in front of the optical fiber to restrict the fluorescence collected only to the perpendicularly polarized component. A photomultiplier (Hamamatsu 1P21) was used as a detector. The signal from the photomultiplier was fed into and amplified with a lock-in amplifier. Fluorescence intensity data were obtained at the fluorescence wavelength of 580 nm.

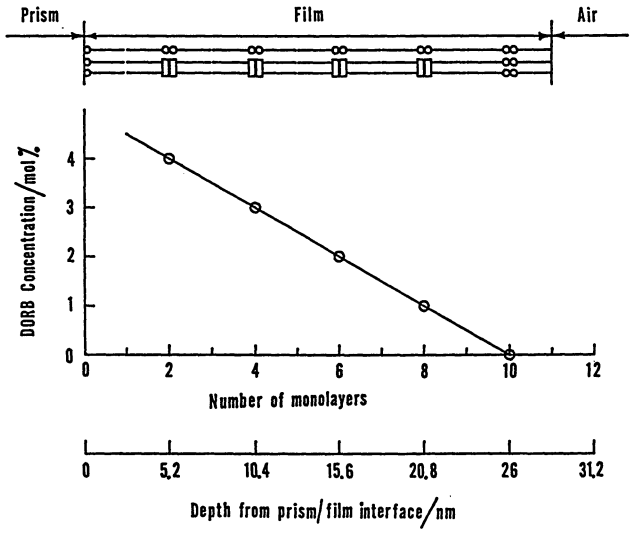

Fig. 3. Concentration depth profile of the model film sample. The upper part is a schematic representation of the model film sample construction. Rectangles represent the head groups of DORB, which are the fluorophores. Circles represent CdC_{20} head groups (nonfluorescent). Long hydrocarbon chains are represented as lines. The lower part is the concentration depth profile represented graphically. The circles and the straight line represent the true and approximate linear function form concentration depth profiles, respectively.

The LB multilayer deposition method was used to prepare a model film sample where $C(z)$ is a nearly linear function form. A model film sample having an exact linear function form or an exponential function form $C(z)$ is difficult to prepare. Details of the preparation procedure were reported previously.[7] The LB multilayers were deposited onto the prism directly. In order to ensure the prism surface was uniform and hydrophobic, a monolayer of CdC_{20} was first deposited. Then a mixture of CdC_{20} and N,N'-dioctadecylrhodamine B (DORB), in which the concentration of DORB varied from 4% to 0%, was deposited in 2 layer steps. The concentration depth profile of the model film sample is shown in Fig. 3, and its $C(z)$ can be precisely expressed as a discrete function with the spacing of a bilayer thickness (5.2 nm) between the values. This concentration depth profile of the model film sample is approximately described as a linear function form in the same manner as the previous report,[7]

$$C(z)(\%) = -0.19(\%\ \mathrm{nm}^{-1})\ z(\mathrm{nm}) + 5(\%). \quad (6)$$

Results and Discussion

In order to obtain $C(z)$ from Eq. 1, the necessary condition is that the partial derivative of $T(\theta, z)$ with respect to z, $\partial T(\theta, Z)/\partial Z$, must not be equal to zero. Otherwise $T(\theta, z)$ is independent of z, that is, $T(\theta, z)$ becomes a constant $T(\theta)$, and Eq. 1 becomes as follows,

$$F(\theta) = kT(\theta)\int_0^t C(z)\mathrm{d}z. \quad (7)$$

It is clear that information on $C(z)$ disappears from the observed $F(\theta)$ expressed in Eq. 7.

Figure 4 shows a calculation example of the relations between $\partial T(\theta, Z)/\partial Z$ and the film thickness at the observation angle of 20°. The calculation results show

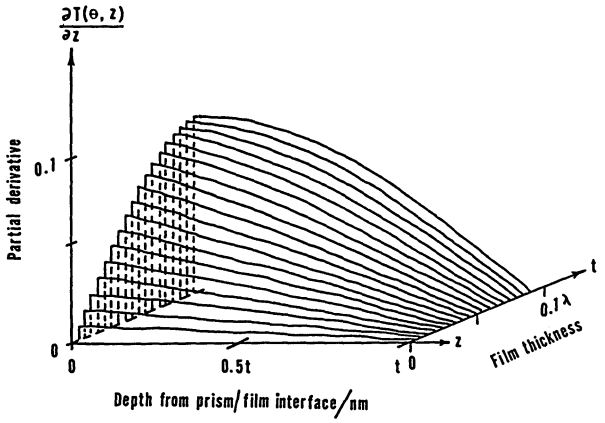

Fig. 4. Calculation results of partial derivative $\partial T(\theta, z)/\partial z$ for different film thicknesses at observation angle 20°. t: film thickness. λ: wavelength of fluorescence.

the partial derivative is not zero, and moreover, $\partial T(\theta, Z)/\partial Z$ has different values at different θ. This means that at different θ_i, $T(\theta_i, z)$ has different function forms. Hence, $C(z)$ can be obtained mathematically from Eq. 1 regardless of t. In other words, theoretically, this method is not limited by the film thickness. It is obvious from Eq. 1 that the measured fluorescence $F(\theta)$ does not involve informations related to concentration distribution $C(z)$ when $\partial T(\theta, Z)/\partial Z$ is zero, even though $T(\theta, z)$ has certain value.

Considering the above theoretical results and the previous experiments,[7] the application limit is considered to depend on instrumental factors and experimental errors. Then, their effects on the accuracy of the reconstructed $C(z)$ were investigated. After that, the application limits of film thickness under our experimental conditions were discussed on the basis of the simulation results.

For the first case in which $C(z)$ is a linear function form, Fig. 5 shows the simulation results of the effects of ϕ, $\Delta\theta$, and ΔF on the accuracy of the reconstructed $C(z)$. The circles and the vertical error bars in Figs. 5-B) and 5-C) represent the average values and variation for ten simulation results taking the values $\theta_i+\Delta\theta$ or $\theta_i-\Delta\theta$, and $F_m(\theta_i)+\Delta F$ or $F_m(\theta_i)-\Delta F$ randomly for Figs. 5-B) and 5-C), respectively. The relative value $\Delta F/F$ in Fig. 5-C) is considered to be the same as the signal to noise ratio (S/N). Since $F_m(\theta)$ takes a value within the range of $F_m(\theta)\pm\Delta F$, the noise is considered as $2\Delta F$. Thus the relation between $\Delta F/F$ and S/N is as follows,

$$\Delta F/F = 1/2(S/N). \tag{8}$$

The vertical axes of Fig. 5 represent the relative error $\Delta B/B$ of the parameter B obtained from Eq. 5 and $\Delta B/B$ decreases with decreasing ϕ. The variation range of

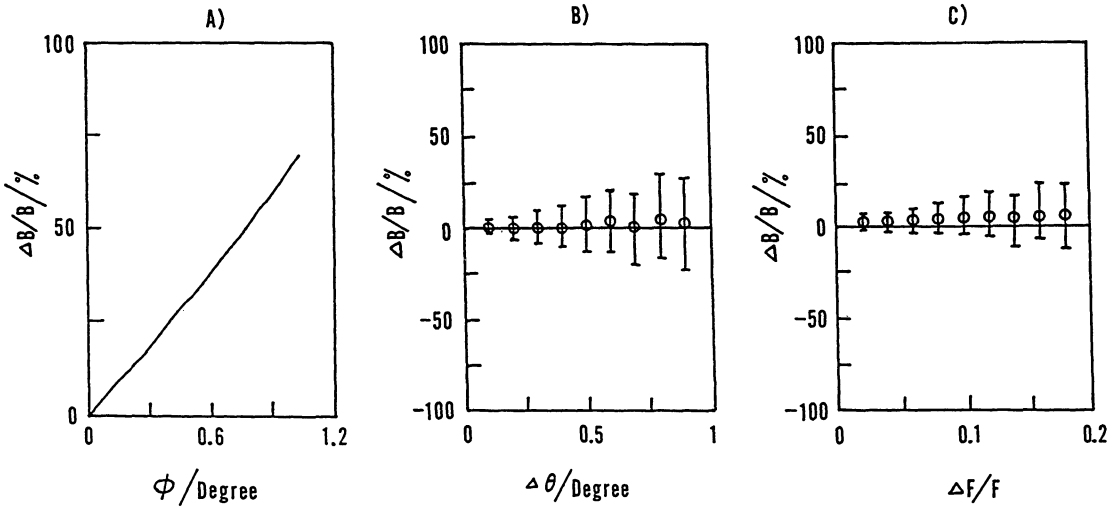

Fig. 5. Effects of instrumental factors on the accuracy of the reconstructed concentration depth profile for the first case. A: effect of ϕ on $\Delta B/B$. B: effect of $\Delta\theta$ on $\Delta B/B$. C: effect of ΔF on $\Delta B/B$.

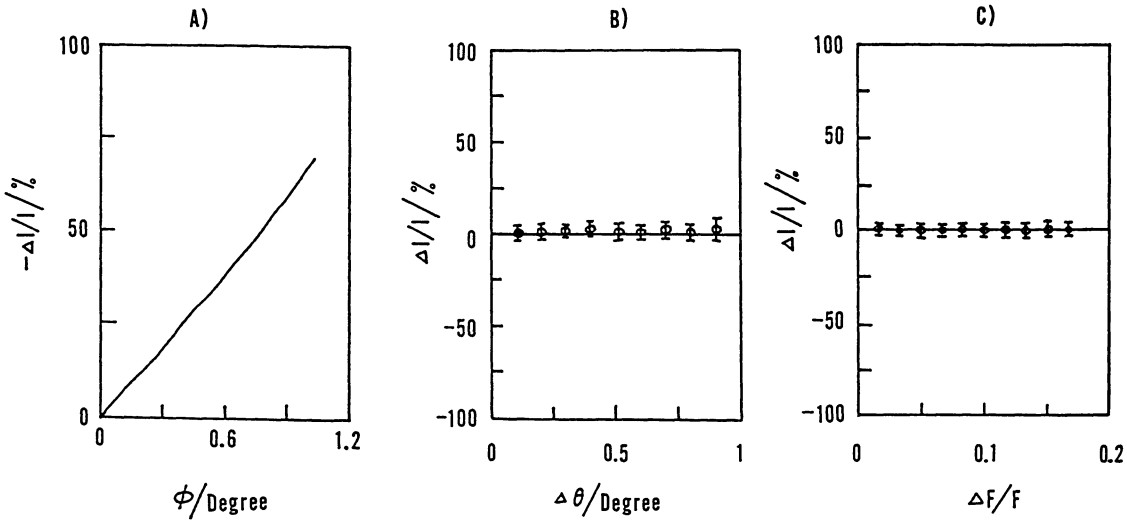

Fig. 6. Effects of instrumental factors on the accuracy of the reconstructed concentration depth profile for the second case. A: effect of ϕ on $\Delta l/l$. B: effect of $\Delta\theta$ on $\Delta l/l$. C: effect of ΔF on $\Delta l/l$.

$\Delta B/B$ also decreases with the decrease of both $\Delta\theta$ and $\Delta F/F$ although the average values of $\Delta B/B$ are nearly equal to zero as shown in Figs 5-B) and 5-C). These results indicate that the accuracy of the reconstructed $C(z)$ depends on the experimental errors. The effects of ϕ, $\Delta\theta$, and ΔF on $\Delta A/A$, which is the relative error of the parameter A of the linear equation function form expressed as Eq. 2, were also simulated and the results are simular to those shown in Fig. 5.

It has been stated that ϕ is determined by the size of the detector, and the distance between the detector and the illuminated point. When using a small sized fiber bundle, ϕ can be decreased, so that accuracy of the reconstructed $C(z)$ can be improved. However, at the same time, S/N decreases which results in a decreased accuracy of the reconstructed $C(z)$. Therefore there is an optimum condition between ϕ and ΔF, which is determined experimentally.

For the second case in which $C(z)$ is an exponential function form, Fig. 6 shows the effects of ϕ, $\Delta\theta$, and ΔF on the accuracy of the reconstructed $C(z)$. It is clear that the relative error $\Delta l/l$ of parameter l in Eq. 3 decreases with decreasing ϕ, but varies hardly at all with $\Delta\theta$ and $\Delta F/F$ in comparison with the first case shown in Fig. 5. For the first and the second cases, Eq. 1 takes the following forms:

$$F(\theta)=k[A\int_0^t zT(\theta, z)\mathrm{d}z+B\int_0^t T(\theta, z)\mathrm{d}z], \quad (9)$$

$$F(\theta)=k\int_0^t c_0 \exp(-z/l)T(\theta, z)\mathrm{d}z. \quad (10)$$

Therefore, the relations between ΔF and ΔA, ΔB and Δl are expressed as Eqs. 11 and 12, respectively.

$$\Delta F=[\Delta A\int_0^t zT(\theta, z)\mathrm{d}z+\Delta B\int_0^t T(\theta, z)\mathrm{d}z], \quad (11)$$

$$\Delta F=k\int_0^t [\exp(-z/(1+\Delta l))-\exp(-z/l)]T(\theta, z)\mathrm{d}z. \quad (12)$$

It can be seen that ΔF has a linear relation with ΔA and ΔB for the first case, but it has an exponential relation with Δl for the second. Thus ΔF has a smaller effect on the exponential distribution than the linear one. When $\Delta\theta$ and $\Delta F/F$ are within the range of 0—1° and 0—0.2, the average values of $\Delta l/l$ in Figs. 6-B) and 6-C) are nearly equal to zero, and the variation range of $\Delta l/l$ is about ±5%. Therefore, in this case, the effects of $\Delta\theta$ and ΔF are small, and ϕ is the main factor affecting the accuracy of reconstructed $C(z)$.

For the third case in which $C(z)$ is an error function form, the effects of ϕ, $\Delta\theta$, and ΔF on the accuracy of reconstructed $C(z)$ were also investigated, and the results are similar with those shown in Fig. 6.

In conclusion, when $C(z)$ is an exponential function form or an error function form, the accuracy of the reconstructed $C(z)$ is mainly determined by the instrumental factor ϕ. When $C(z)$ is a linear function form, the accuracy of the reconstructed $C(z)$ depends on both the instrumental factors ϕ and $\Delta\theta$, and the experimental ΔF. However, if $\Delta\theta$ is smaller than 0.05° and S/N is above 10, $\Delta B/B$ caused by $\Delta\theta$ and ΔF are estimated to be about ±1% and ±4% respectively from Figs. 5-B) and 5-C). Under this situation, ϕ is also the main factor for affecting the linear distribution.

Figure 7 shows the simulation results of the relations between $\Delta B/B$ and film thickness t. The relations between $\Delta l/l$ and the film thickness t for the exponential and error function cases are similar to those shown in Fig. 7. The plotted data indicate that $\Delta B/B$ increases with thinner films. In other words, the accuracy of the reconstructed $C(z)$ becomes worse when the film thickness decreases. For an experimental system, ϕ has a fixed value, thus the applicable limit of film thickness can be obtained according to the required accuracy of the reconstructed $C(z)$, although there is no limitation theoretically. For example, to keep $\Delta B/B$ smaller than ±10%, when ϕ is 0.3°, the limit of film thickness is about 50 nm from Fig. 7.

In our experiment, the accuracy of the rotating stage was 0.05°, and signal to noise ratio was kept above 10. The fiber bundle width was about 0.2 mm, and the distance between the fiber bundle and the illumination point was about 21.4 mm. Thus ϕ is calculated to be 0.13°. The errors of the reconstructed $C(z)$ caused by $\Delta\theta$ and ΔF are estimated to be ±1% and ±4% from Figs. 5-B) and 5-C), respectively. The errors of reconstructed $C(z)$ caused by ϕ, $\Delta\theta$, and ΔF are a cumulative error. Therefore, in order to maintain an accuracy of the reconstructed $C(z)$ of better than 10%, the error of the reconstructed $C(z)$ caused by ϕ must be smaller than ±5%. For this accuracy level and the value of ϕ, the limitation of film thickness is estimated to be about 30 nm from Fig. 7. This theoretical analysis result is verified by the experiments using the 29 nm thick LB model film sample.

Figure 8 shows the experimental and theoretical fluorescence intensity dependence on the observation angle under normal incidence conditions for the model film sample. The theoretical and experimental results are represented by a solid line and circles, respectively. The theoretical values were obtained by substituting

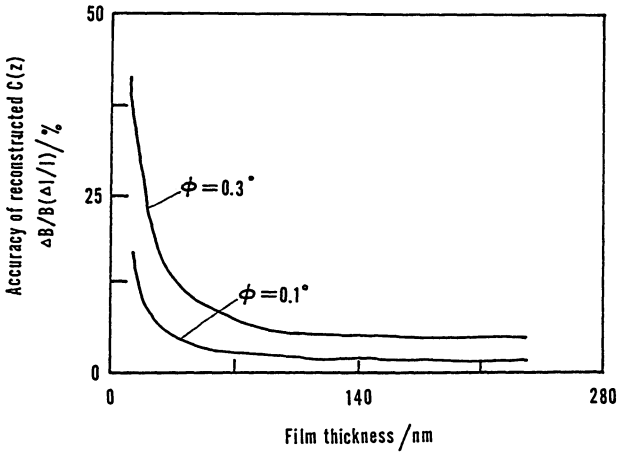

Fig. 7. Dependence of the accuracy of the reconstructed concentration depth profile on film thickness for the case that $C(z)$ is a linear function form.

$C(z)$ expressed as Eq. 6 into Eq. 1. The theoretical values agree well with the experimental ones.

With the fluorescence intensity data presented in Fig. 8, the constants A and B of the linear function form used as the test function were calculated from Eq. 5. Figure 9 shows the results of the reconstructed $C(z)$ with the actual $C(z)$ described in circles. The solid and dotted lines represent the average reconstructed $C(z)$ and its variation range for four times determinations, respectively. The average values calculated for the parameters A and B are -0.21% nm $^{-1}$ and 5.48%, respectively. As shown in Eq. 6, the values of A_0 and B_0 of the model film sample are approximately -0.19 (% nm^{-1}) and 5 (%), respectively (Fig. 3). Hence $\Delta A/A$ and $\Delta B/B$ are got as 10.5% and 9.5%, respectively. Therefore the accuracy of reconstructed $C(z)$ is about 10% which agrees well with the theoretical estimation. The model film sample consists of long chain molecular bilayers, and the concentration changes in each bilayer have been recognized with a reasonable accuracy as shown in Fig. 9. Hence the spatial resolution in the depth direction is estimated to be at least on the order of the bilayer thickness, 5.2 nm.

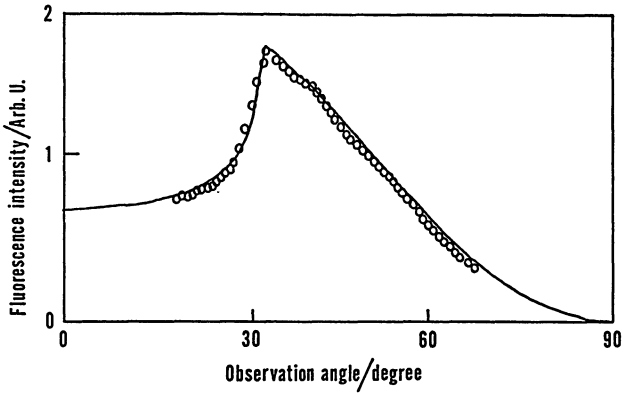

Fig. 8. Theoretical and experimental results of the angular dependency of the fluorescence intensity measured for the model sample. The theoretical values are described by the solid line, and the experimental results are plotted with circles.

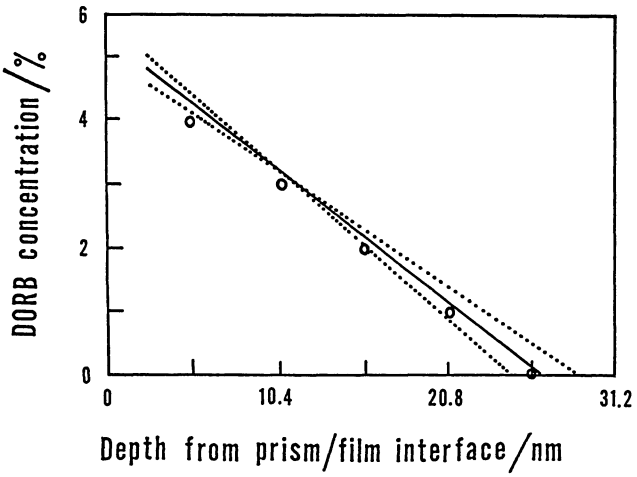

Fig. 9. Reconstructed concentration depth profile for the model film sample. The solid and dotted lines represent the average reconstructed $C(z)$ and the variation range of reconstructed $C(z)$. The circles represent the actual $C(z)$ of the model sample.

The signal to noise ratio can be improved using a more sensitive photomultiplier. For example, a photomultiplier such as Hamamatsu R923 is more sensitive by a factor of 5 than the used one in our experiments (Hamamatsu 1P21). Moreover, it can be improved further by using a photon counting technique. Therefore, the signal to noise ratio can be improved at least by a factor of 10 compared with our present experiments. This means ϕ can be decreased by a factor of 10, then the limitation of the film thickness is estimated to be 5 nm from Fig. 7, and concentration depth profiles on the nm level or molecular level are expected. In fact, Fig. 9 suggests, where the molecule is a long chain molecule, that the concentration depth profile is on the molecular level.

The authors wish to express their thanks to Professor Y. Goshi and Dr. K. Miyamura of the University of Tokyo, for their useful advice in preparation of the model LB film sample.

References

1) D. L. Taylor and Y-L. Wang, "Fluorescence Microscopy of Living Cells in Culture, Pt. B: Quantitative Fluorescence Microscopy-Imaging and Spectroscopy," "Methods in Cell Biology," Academic Press, Inc., London (1989), Vol. 30.

2) E. Kaneko, H. Tanno, and T. Yotsuyanagi, *Mikrochim. Acta,* **III**, 333 (1988).

3) A. Harata and T. Sawada, *J. Appl. Phys.*, **65**, 959 (1989).

4) T. Hirschfeld, *Appl. Spectrosc.*, **31**, 289 (1977).

5) P. W. Bohn, *Anal. Chem.*, **57**, 1203 (1985).

6) D. R. Miller, O. H. Han, and P. W. Bohn, *Appl. Spectrosc.*, **41**, 245 (1987).

7) X-Z. Wu, T. Kitamori, N. Teramae, and T. Sawada, *Bull. Chem. Soc. Jpn.*, **64**, 755 (1991).

8) P. A. Suci and W. M. Reichert, *Appl. Spectrosc.*, **42**, 120 (1988).

9) P. A. Suci and W.M. Reichert, *Lanqmuir,* **4**, 1131 (1988).

10) D. R. Miller and P. W. Bohn, *Anal. Chem.*, **60**, 407 (1988).

11) T. Albert, "Inverse Problem Theory," Elsevier, New York (1987).